DNN-Based Approach to Mitigate Multipath Errors of Differential GNSS Reference Stations

Dongchan Min, Minchan Kim, Jinsil Lee, Mihaela Simona Circiu, Michael Meurer, and Jiyun Lee

***Abstract*— One of the major error components of differential global navigation satellite systems is a multipath error in a reference station. This paper introduces a deep neural network based multipath modeling method. A signal to noise ratio, as well as satellite geometry, is used as a feature parameter to capture the variation of the multipath error caused by unavoidable changes in the vicinity of the reference station. The performance of the proposed method is demonstrated for both normal and varying multipath cases using experimental data. The remaining multipath error after mitigation is well bounded by the standardized error model.**

***Index Terms*— Differential global navigation satellite system, deep neural network, multipath error mitigation.**

I. Introduction

Adifferential global navigation satellite system (GNSS) technique, which generates range error corrections from reference stations at fixed and known locations is widely used to improve positioning accuracy. Not only is accuracy improved by this technique, but with monitoring functions it can detect and exclude satellite faults or other anomalies in the transmitted signals before they affect users [1]. Differential GNSS (DGNSS) with such augmentation allows navigation systems to provide sub-meter accuracy and high level of integrity. Thus, DGNSS will be a key component of future air transportation systems (e.g., urban air mobility) to help meet the demanding navigation requirements [2].

One of the dominant error sources of DGNSS is a multipath error of the reference station. The multipath error occurs when the signal arrives at the antenna from reflecting surfaces (e.g., the ground and structures in the vicinity) in addition to the line-of-sight source. The multipath errors at a DGNSS reference station and aircraft are mostly uncorrelated, and thus the correction process cannot remove the multipath error. Because the multipath environment of the reference station can be considerably more severe than that of the aircraft, it is of particular interest to reduce the multipath error in the reference station. The reference station should be installed in an open-sky area as free from reflecting objects as possible to ensure DGNSS accuracy and integrity against multipath errors. The siting criteria, however, cannot completely remove multipath signals due to the ground or objects around the vicinity of antennas.

The problem of mitigating multipath error in pseudorange measurements has received considerable research attention. The most commonly used methods are attenuating the multipath signals at the antenna or receiver level. The antennas were designed to be less sensitive to the reflected signals [3]. The development effort yielded a multipath limiting antenna (MLA) which uses a vertical array of dipole elements [4], [5]. Multipath mitigation techniques at the receiver level use a modified discriminator to improve the resolution of the signal correlation process [6], [7], [8], [9]. Recently, several studies have adopted a machine learning (ML) technique to attenuate the multipath signals. In [10], [11], and [12], the ML-based angle-of-arrival estimation was used for a multipath signal discrimination from incoming signals, and in [13], a neural network-based delay-locked loop was proposed. These advanced antennas and receivers significantly reduce multipath errors; however, they cannot completely eliminate such errors and the applications of some of those techniques are expensive.

An alternative is to estimate and correct the multipath error at the measurement level. One of the fundamental techniques is a carrier smoothing filter (CSF) [14], but a gradually varying multipath error cannot be smoothed. The multipath error can be predicted from a known receiver environment and the laws that govern the propagation of electromagnetic radiation [15], but it is computationally intensive. The other approach is empirical modeling. For the antenna installed in an essentially static environment, the repeating satellite geometry of the GNSS constellation produces repeating multipath effects. The multipath error on the currently visible satellite, therefore, is identified and used to correct measurements on the subsequent repeating period. This is referred to as sidereal filtering or daily filtering in the community [16], [17], [18]. Another empirical modeling method is to map the multipath errors onto a sky plot, which is called space-domain modeling [19], [20], [21], [22]. The ML-based models were also developed, which use the elevation and azimuth angels [23], [24] or GNSS coordinates series [25] as input parameters.

The assumption made in these empirical modeling approaches is that the vicinity of the reference station is ideally well-maintained; for example, the placement of the reflecting object remains constant and its reflective properties do not change. However, changes in the reflective properties are inevitable due to variables affecting them, such as temperature, humidity, or precipitation. For instance, after a rain fall, the reflecting properties of the surfaces of the reflecting objects may change, resulting in a variation of multipath signals. These reflected signals have a different intensity or phase compared with the reflected signals from dry surfaces, which causes different multipath errors.

The goal of this work is to capture and estimate the variation of multipath errors caused by inevitable changes of an antenna environment. The day-to-day variation of the multipath errors is presented to show the degree to which precipitation affects the

Manuscript received 30 November 2021; revised 3 July 2022; accepted 13 September 2022. Date of publication 28 September 2022; date of current version 5 December 2022. This work was supported in part by the Ministry of Science and ICT (MSIT), Korea, under the High-Potential Individuals Global Training Program (No. 2020-0-01531) supervised by the Institute for Information & Communications Technology Planning & Evaluation (IITP); and in part by the National Research Foundation of Korea (NRF) grant funded by the Korean Government (MSIT) (No. 2020R1A2C1011745). The Associate Editor for this article was Z. M. Kassas. *(Corresponding author: Jiyun Lee.)*

Dongchan Min and Jiyun Lee are with the Department of Aerospace Engineering, Korea Advanced Institute Science and Technology, Daejeon 34141, South Korea (e-mail: willy1994@kaist.ac.kr; jiyunlee@kaist.ac.kr).

Minchan Kim and Jinsil Lee were with the Department of Aerospace Engineering, Korea Advanced Institute Science and Technology, Daejeon 34141, South Korea. They are now with the Korea Positioning System R&D Directorate, Korea Aerospace Research Institute, Daejeon 34133, South Korea (e-mail: minchankim@lx.or.kr; jinsil.lee@dlr.de).

Mihaela Simona Circiu was with the German Aerospace Center, Navigation Department, Oberpfaffenhofen, 82234 Wessling, Germany. She is now with the European Space Agency, 2201 Noordwijk, Netherlands (e-mail: mihaela-simona.circiu@dlr.de).

Michael Meurer is with the German Aerospace Center, Navigation Department, Oberpfaffenhofen, 82234 Wessling, Germany (e-mail: michael.meurer@dlr.de).

Digital Object Identifier 10.1109/TITS.2022.3207281

Fig. 1. Antenna configuration at Station NYLP [27].

TABLE I
RECEIVER/ANTENNA INFORMATION OF CORS STATIONS

Station ID	Receiver	Antenna	Location
NYIL	LEICA GRX1200GGPRO	LEIAT504GG	Indian Lake, NY
NYLP	LEICA GRX1200+GNSS	LEIAR10	Lockport, NY
TXAU	TRIMBLE NETR9	TRM55971	Austin, TX
ROD1	TRIMBLE NETR9	TRM55971	Spring, TX
TXAN	TRIMBLE NETR9	TRM55971	San Antonio, TX

multipath errors. The proposed method uses signal to noise ratio as one of the feature parameters to capture the variation and employs deep neural networks (DNN) to construct the empirical model of multipath errors.

This paper presents the experimental results obtained by using the data observed at five different reference stations. In addition, it compares the standard deviations of the corrected multipath errors with the ground accuracy designator of a ground based augmentation system (GBAS) under the assumption that GBAS will be applied for future air transportation systems. The final section summarizes this paper and suggests future efforts. This paper is an expanded version of an earlier conference publication [26], including new experimental results using continuously operating reference stations (CORS) data.

II. DATA USED FOR THE ANALYSIS

The data collected at CORS stations were used to evaluate the performance of the DNN-based multipath error modeling. The CORS stations provide collected GNSS data throughout the United States, its territories, and a few other countries, which are publicly available at [27]. The CORS stations are sited in an open area where there are no obstructions 10 degrees above the horizon [28]. Five CORS stations, for which weather databases are available at [29], were chosen to examine the relationship between the variation of multipath error and the precipitation. Their station ID, installed GNSS equipment, and location are listed in Table I. Fig. 1 shows the antenna configuration at Station NYLP as an example [27]. The data from day of year (DOY) 113–143 in 2019 and 61–81 in 2020 were used for the performance evaluation. We extracted the multipath errors from the GNSS code-phase pseudorange measurements using the method proposed in [23] and implemented the CSF [14] with a smoothing time constant of 100 s. The receiver thermal noise was assumed negligible after applying the CSF.

III. MULTIPATH ERRORS AND SIGNAL TO NOISE RATIO

Multipath is caused by signals arriving at an antenna via multiple paths, as depicted in Fig. 2. The primary path is a direct path from the satellite to the antenna (i.e., line-of-sight). In contrast, the secondary paths are reflections of the nearby objects or ground [3]. The reflected

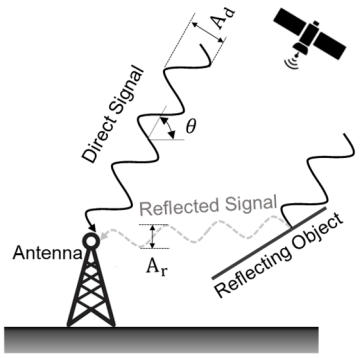

Fig. 2. Illustration of multipath signal.

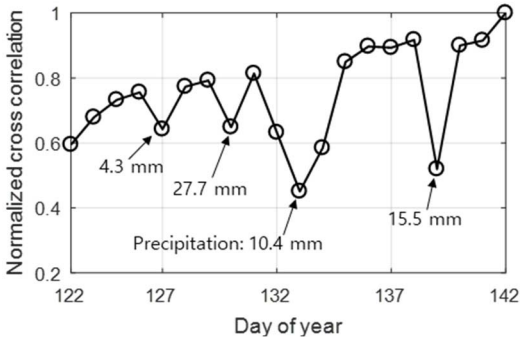

Fig. 3. Normalized cross-correlation of the multipath errors (dates) and the corresponding precipitation.

and delayed signal corresponds to a weaker version of the direct signal [3]. When the direct signal is combined with the reflected signals, the signal modulation is distorted. This causes the receiver to struggle in estimating the true arrival time of the direct signal, inducing the multipath error in the pseudorange measurement.

The multipath signals can be characterized in terms of amplitude, time delay, and phase relative to the direct signal. The multipath error is proportional to the relative strength of the multipath signal, and nonlinearly varies as a function of time delay and relative phase [30]. The time delay of a given multipath signal is entirely dependent upon the geometry of the environment in which the receiver is located. The amplitude and phase rely on both the environment and the characteristics of the user's antenna and receiver. In the case of a stationary antenna, the multipath error on a pseudorange measurement can, therefore, be modeled as a function of the azimuth and elevation angles of the corresponding satellite, unless there are changes in the nearby objects. However, in practice, even if the vicinity of the antenna is well maintained, the multipath error is not free from its daily variation due to both slow and rapid changes of the surrounding environment.

The day-to-day variation of the multipath errors for consecutive days can be demonstrated by evaluating their cross-correlation. Fig. 3 shows the normalized cross-correlation between the multipath error sequence of DOY 142 and the sequence of the dates within DOY 122–142. The GNSS measurements collected at the NYIL station were used for this correlation analysis. As presented in Fig. 4, the normalized cross-correlation of each date decreases as the time gap from DOY 142 increases, due to the increased variation in the multipath errors. The variations can be classified into two categories: a slow and continuous variation, and a rapid and temporary variation. The variation grows slowly and continuously as the cumulative environmental changes become inevitable over time, even though the environment is properly maintained.

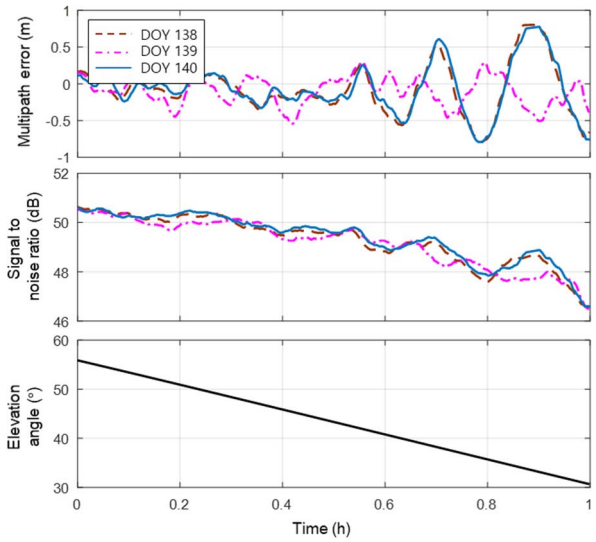

Fig. 4. Multipath error and signal to noise ratio aligned with its satellite elevation angles on three consecutive days.

The rapid and temporary variation in the multipath error represents an unexpected and impermanent change in the vicinity of the antenna. There could be various factors which produce abrupt changes in the surrounding environment for a short time. One of the most common and inevitable causes is precipitation, which includes rain, sleet, frost, and more. After rains, the reflecting objects are wet and this causes the reflecting surfaces to have different reflecting properties in comparison with a dry surface. This changes the amplitude, phase, and time delay of the reflected signals. These changes disappear once the surfaces completely dry. The example relationship between precipitation and multipath is shown in Fig. 3. Four rapidly and temporarily decreasing cross-correlations occur on DOY 127, 130, 133, and 139, and their precipitations are 4.3, 27.7, 10.4, and 15.5 mm, respectively. This variation cannot be captured by previous efforts [16], [17], [18], [19], [20], [21], [22], [23], [24], [25], which only rely on the repeatability of the satellite geometry to estimate the multipath error. Therefore, an additional parameter is required to detect the changes of the surrounding environment inducing the variation of the reflected signals.

This study utilizes the signal to noise ratio (SNR) value of the incoming signal as a feature parameter to capture the variations of the multipath signals. In [31], the SNR value was used to adaptively estimate the spectral parameters (e.g., A_i, ψ_i) of multipath signals. The SNR of the multipath signals can be expressed, as in (1), for a case where a direct signal is combined with n multipath signals [31]

$$SNR_{MP} = \sum_{i=1}^{n} A_i \cos(\psi_i) + \varepsilon \tag{1}$$

where SNR_{MP} is the SNR values of the multipath signals, A_i represents the amplitudes of the reflected signals, and ψ_i is the argument directly related to the relative phase of the multipath signals. ε is the noise term. The changes in the reflective properties of the reflecting objects produce variations in A_i and ψ_i, resulting in a difference in the SNR value. In Fig. 4, the multipath errors and SNR values of DOY 138, 139, and 140 are plotted in accordance with their satellite elevation angles, using the NYIL station data. The precipitations on those dates were 0, 15.5, and 1.8 mm per day, respectively [29]. The precipitation on DOY 139 changes the reflective properties of the reflecting object, and thus the SNR values of DOY 139, as well as the multipath errors, show different sequences, compared with those of DOY 138 and DOY 140. This yields a possibility of capturing the multipath errors resulting from the precipitation by utilizing the SNR value which is available at the receiver.

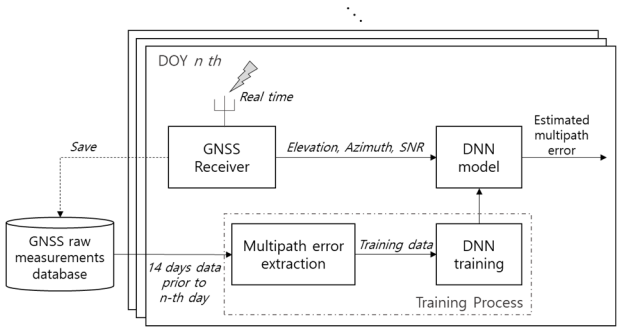

Fig. 5. Schematic representation of the proposed DNN-based multipath error mitigation method.

The use of SNR values and the satellite geometry (i.e., the azimuth and elevation angles) as feature parameters makes the model construction problem more complex than the case of relying on the satellite geometry only. One of the important aspects of the empirical modelling technique is the algorithm used to construct the model. In [32], it was rigorously established that a standard multilayer feedforward network, which is the DNN, is capable of approximating the function of interest to any desired degree of accuracy, provided that sufficient number of hidden units are available. DNN has been extensively used in many applications (e.g., signal processing, pattern recognition) to approximate complex nonlinear systems, and its considerable results have been reported in the literature [33], [34]. Thus, a new DNN-based multipath error modeling method is proposed in the following section.

IV. DNN-Based Multipath Mitigation Method

This study proposes a DNN-based multipath error modeling method for the DGNSS reference station. The reference station was assumed to be well maintained to prevent any environmental changes near the antenna, except for inevitable causes including a long-term seasonal variation or precipitation. The satellite elevation and azimuth angles and the SNR value are used as input features of the DNN model, and the DNN outputs the corresponding multipath error. The satellite elevation and azimuth angles, used for determining the traveling paths of the signals, contain information regarding the time delays of the reflected signals. The SNR value includes information on the amplitude and phase of the reflected signals.

The schematic layout of the proposed system architecture is depicted in Fig. 5. The GNSS raw measurement collected from the reference station is stored in a database on each day. These measurements are post-processed to extract the multipath errors, detailed in [23], and are used as training data. The DNN models for each satellite are replaced every day with the newly trained model using the data that are composed of the multipath errors observed from a series of previous dates to the present. The period of the training data shall be long enough to contain information with which the DNN can learn the relationship between the input features and the multipath error. However, if the period is too long, the training data might contain the multipath error which has little correlation with the current multipath error due to the slow and continuous environmental changes. This causes a degradation of the performance of the DNN. Thus, the period should be tuned depending on the surrounding environment of the antenna. We evaluated the performance of the DNN while gradually increasing the period of the training data and set it as 14 dates for the selected CORS station. In practice, the same

or similar approach needs to be conducted to search for an optimal window size of training data before initiating the system.

A 'tanh' function was used as an activation function of the DNN model, and a Levenberg-Marquardt algorithm was used to optimize the DNN using the mean squared error as the loss function. We set up two hidden layers and 20 hidden nodes for each layer, which were determined to achieve acceptably low validation errors by trying different layer (from one to ten) and node per layer (from two to fifty) combinations. We also tested recurrent neural networks (RNN), but they took approximately ten times longer training time than DNNs while the performance was improved by only about two percent. Thus, we chose the DNN by considering a trade-off between better performance and less computational time.

V. Performance Evaluation

The DNN-based multipath error mitigation method is compared with the daily filter method proposed in [16]. We use the reduction rate of the multipath error standard deviation as the performance index, which is defined as

$$r = \frac{\sigma_{true} - \sigma_{corrected}}{\sigma_{true}} \times 100, \tag{2}$$

where σ_{true} and $\sigma_{corrected}$ represent the standard deviations of the true and corrected multipath errors, respectively. The corrected multipath error is the residual error, which is defined as

$$MP_{corrected} = MP_{true} - MP_{estimated}, \tag{3}$$

where MP_{true} is the true multipath error obtained after applying a 100-seconds smoothing filter, and $MP_{estimated}$ is the estimated multipath error by the DNN or daily filter.

The daily filter method is an intuitive and powerful method to mitigate multipath errors of reference stations. However, its performance is degraded when today's multipath error changes from that of yesterday. Thus, the performance comparisons between the DNN and the daily filter were conducted for two cases: a normal case and a variation case.

1) *Normal Case*: today's multipath error is almost the same as that of yesterday.
2) *Variation Case*: today's multipath error is different from that of yesterday.

In the normal case, as the two multipath error sequences on consecutive days are similar to each other, the reduction rate obtained using the daily filter could be high in comparison with that in the variation case. We categorized the dates used for the evaluation into the two cases for each station based on the daily filter reduction rate. Assuming that the number of days in the normal case is larger than that of the variation case, the thresholds categorizing the two cases were determined from the median and median absolute deviation (MAD) of the reduction rate obtained by using the daily filter. The detailed procedure is as follows:

1) Compute the reduction rate ($r_s^{j,i}$) of the *j-th* satellite, *i-th* day, and station s using the daily filter;
2) Compute the averaged reduction rate (r_s^i) of the *i-th* day and station s:

$$r_s^i = \frac{1}{n_{sat}} \sum_{j=1}^{n_{sat}} r_s^{j,i}, \tag{4}$$

where n_{sat} indicates the number of satellites.

3) Calculate the median of the averaged reduction rate of the station s ($\tilde{r_s}$) and compute its MAD_s, as follows:

$$\tilde{r}_s = \underset{i}{\text{median}}\, r_s^i, \tag{5}$$

$$MAD_s = \underset{i}{\text{median}} \left(\left| r_s^i - \tilde{r}_s \right| \right). \tag{6}$$

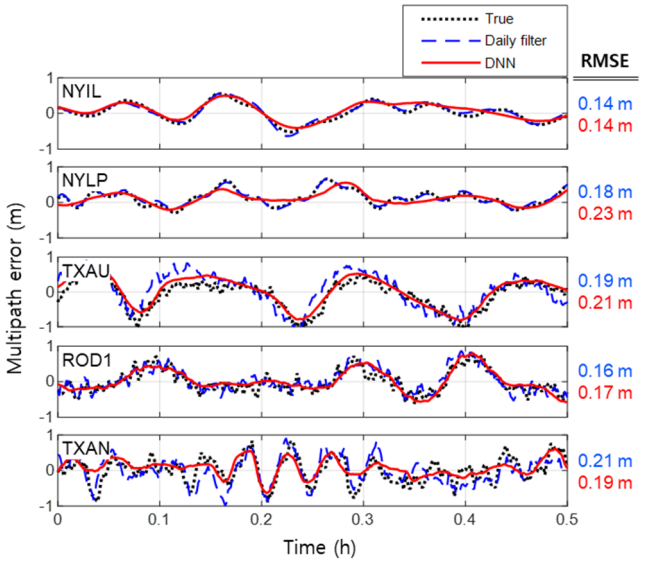

Fig. 6. True multipath errors and those estimated by the daily filter and DNN for the normal case for the five stations. The root mean square errors of the daily filter (blue) and DNN (red) are given at the right-hand side for each station.

4) Classify the *i-th* day of station s into:

$$\text{Normal case} \quad \text{if } r_s^i \geq \tilde{r}_s - MAD_s,$$
$$\text{Variation case} \quad \text{if } r_s^i < \tilde{r}_s - MAD_s.$$

For this study, as the DNN training process requires a period of 14 dates for the training data, the dates within the period of DOY 127–143 in 2019 and DOY 75–81 in 2020, not the entire period, were classified and used for the performance analysis

A. Normal Case

Fig. 6 plots the true multipath errors (black dotted line) observed at the five stations on DOY 143, which are classified as normal cases. The figure also shows the estimated multipath errors by the daily filter (blue dashed line) and DNN (red solid line), respectively, and their root mean square errors. At the NYIL and NYLP stations, the true multipath errors oscillate slowly, and the estimated multipath errors from the daily filter are almost the same as the true multipath errors. In contrast, the multipath errors at the TXAU, ROD1, and TXAN stations have high-frequency components in addition to the low-frequency components. The high-frequency components of the multipath induced slight discrepancies between the true multipath error and the estimated error from the daily filter, which degraded the performance of the daily filter.

There could be various factors that produce a difference in multipath characteristics. The major cause of the difference among the selected stations is the GNSS equipment, listed in Table I. The NYIL and NYLP stations use antennas and receivers from manufacturers that are different from those of the TXAU, ROD1, and TXAN stations. Each receiver is equipped with the manufacturer's patented signal tracking algorithms to acquire the pseudorange measurements from the GNSS signals. The receivers of NYIL and NYLP stations are designed to use a high precision pulse aperture multipath correlator [35], and those of TXAU, ROD1, and TXAN are based on high precision multiple correlators [36]. The antenna installed at NYIL is a choke ring antenna, and that of NYLP is a patched antenna equipped with an antenna radome. Those of TXAU, ROD1, and TXAN are patched antennas. The difference between the receiver and antenna designs causes the difference in the multipath characteristics.

TABLE II
MULTIPATH ERROR REDUCTION RATES FOR NORMAL CASE

(Unit: %)		NYIL	NYLP	TXAU	ROD1	TXAN	Total
# of days		18	21	17	21	21	98
DNN	Mean	42.22	31.80	33.73	28.54	24.79	31.84
	Std.	10.11	9.65	7.27	5.68	5.39	6.62
Daily Filter	Mean	49.31	43.36	35.49	27.26	18.57	34.42
	Std.	12.86	15.31	8.91	7.09	7.68	12.42

The performance of the DNN model was compared with that of the daily filter in terms of the reduction rate of the multipath error standard deviation. Table II presents the mean reduction rates over the dates classified as the normal case and their standard deviations. At the NYIL and NYLP stations, where the multipath errors oscillate slowly, the reduction rates obtained using the daily filter are higher than those obtained using the DNN. As the low-frequency component of the multipath error is highly correlated with that of the previous day, the daily filter outperforms the DNN that was trained using the data containing lesser correlated days as the time span increases. In contrast, the mean reduction rates obtained using the daily filter are similar or worse than those obtained using the DNN at the TXAU, ROD1, and TXAN stations, which exhibit the high-frequency multipath errors. This is because the high-frequency components in both the true multipath error and that estimated by the daily filter behave like noises and degrade the mean reduction rates. Unlike the daily filter, because the DNN only outputs the low-frequency component of multipath errors that can be captured by the input features, its adverse effect of subtracting the noise-like error from true multipath was less than that of the daily filter.

As presented in Table II, the standard deviations of the reduction rate when using the DNN are smaller than those when using the daily filter at all stations. This shows that the slight multipath error changes (considerably lesser than the variation case) are also captured by the SNR values. From the entire normal cases, the total mean reduction rate obtained using the DNN is slightly lower than that obtained using the daily filter by 7.5%. In contrast, the standard deviation of the reduction rate of the DNN is smaller than that of the daily filter by 46.70%, which indicates the performance of the DNN is more consistent than the daily filter.

B. Variation Case

Fig. 7 presents the true and estimated multipath errors for the variation case at each station. Similar to the normal case, the TXAU, ROD1, and TXAN stations shows both the low-frequency and high-frequency changes in the multipath errors, whereas the NYIL, and NYLP stations show only the low-frequency components. Because the stations are placed at different locations, the dates classified as the variation case for each station are also different. Fig. 7 plots the data on DOY 130 for the NYIL and NYLP stations, DOY 129 for the TXAU and TXAN stations, and DOY 131 for the ROD1 station. The weather history recorded by [37] indicates that it rained at each station on these dates, with a precipitation of 0.3 – 27.7 mm per day. In Fig. 7, the multipath error of the variation case shows a different time series from that of the previous day, which is equivalent to the multipath error estimated by the daily filter. We cannot be sure of the exact reason for this variation; however, it is very likely that the rain may have produced differences in the reflective properties of the reflecting objects and resulted in the variation of the multipath error. As the daily filter simply shifts yesterday's multipath error by the orbit period of each satellite, it cannot capture the multipath

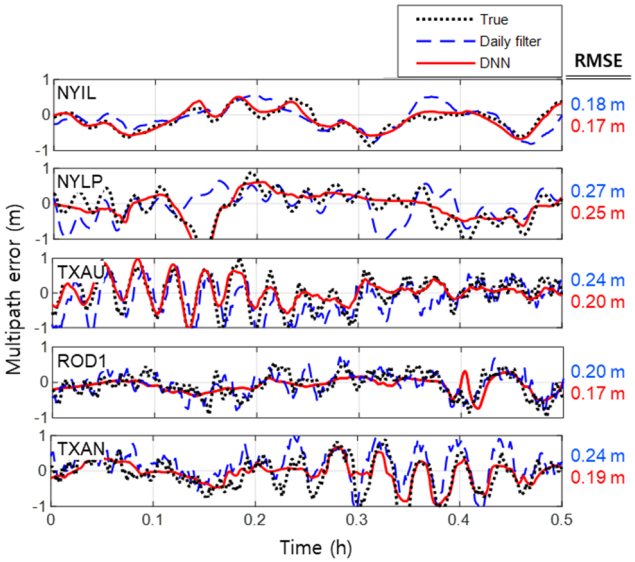

Fig. 7. True multipath errors and those estimated by the daily filter and DNN for the variation case for the five stations. The root mean square errors of the daily filter (blue) and DNN (red) are given at the right-hand side for each station.

TABLE III
MULTIPATH ERROR REDUCTION RATES FOR VARIATION CASE

(Unit: %)		NYIL	NYLP	TXAU	ROD1	TXAN	Total
# of days		6	3	7	3	3	22
DNN	Mean	38.30	26.73	21.11	25.90	23.61	27.48
	Std.	10.27	9.56	7.38	6.08	5.08	7.88
Daily Filter	Mean	29.24	23.65	3.90	18.20	8.62	16.00
	Std.	13.02	13.12	9.57	6.94	7.34	11.27

variation which occurs today, decreasing its multipath error reduction rates. In contrast, the DNN learns the relationship between the input features and the multipath error from the training data; thus, the DNN estimates the multipath error variation. Although the multipath error estimated by the DNN (red solid line) is not perfectly accurate, it is closer to the true multipath error (black dotted line) than that estimated by the daily filter (blue dashed line), as shown in Fig. 7.

The reduction rates obtained using the DNN and daily filter are tabulated in Table III for each station. When using the DNN, the mean reduction rates are higher than those obtained using the daily filter, with an improvement of 13.02% (min.) – 441.28% (max.) at each station. The DNN outperforms the daily filter by 71% in terms of the total mean reduction rate over the five stations and produces a more consistent performance by reducing its standard deviation by 30.08%.

VI. MULTIPATH ERROR MODEL

In this section, the DNN based multipath mitigation method is evaluated and compared with the daily filter by deriving multipath error models for an example GBAS application to future air transportation systems, such as urban air mobility or unmanned aerial vehicles. The GBAS is the DGNSS architecture standard for civil aircraft precision approach and landing navigation under all weather conditions. The current GBAS reference station installs expensive antennas and requires careful siting within a well-controlled airport to achieve its full performance. However, the GBAS variants for future air transportation, which requires many landing sites, may not have the luxury of installing expensive equipment or meeting

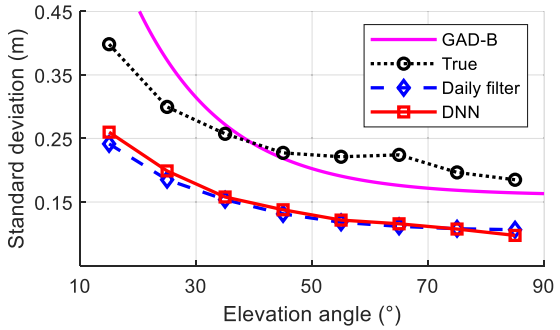

Fig. 8. Multipath error models as a function of the satellite elevation angle. This result was computed using the normal cases of the selected five stations.

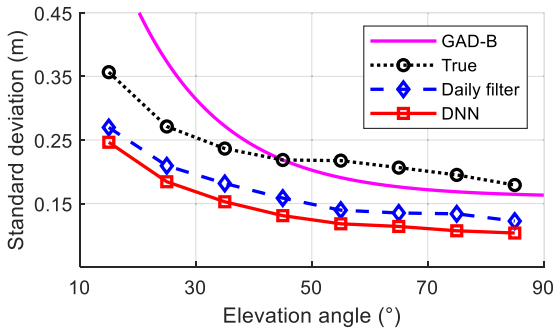

Fig. 9. Multipath error models as a function of the satellite elevation angle. This result was computed using the variation cases of the selected five stations.

siting constraints. Therefore, the use of the daily filter or DNN shall be effective to reduce the multipath errors of their reference stations.

The standardized GBAS error models assume that the pseudorange error components have a zero-mean normal distribution. The standard deviation of the ground multipath component and the receiver noise is classified by the three ground accuracy designators (GAD); A, B, and C, which are associated with the performance type of antenna and receiver. As an intermediate level of performance, GAD-B is defined to represent installations whose performance could be achieved with advanced receiver technologies and conventional antennas [37]. We assume that the future GBAS variants are likely to install antennas and receivers of the GAD-B level, also similar to CORS stations listed in Table I. We, therefore, compare the standard deviation of the multipath errors of the CORS stations with the GAD-B. However, the CORS stations do not meet airport siting requirements, and thus their multipath errors are expected to be greater than those of the GAD-B Model. Note that, because the GAD model is used for the airborne positioning algorithm and integrity protection level computations, the true standard deviations must be equal to or smaller than the GAD model.

The standard deviations of the remaining multipath errors after mitigation were computed for the CORS stations as follows. We collected the corrected multipath error data from all satellites and all stations. Then, we sorted the collected data into satellite elevation bins of 10 degrees, and computed the sample mean and sample standard deviation of the corrected multipath errors for each bin. The standard deviation used for the comparison with the GAD-B model was computed by adding the sample standard deviation and the absolute value of sample mean for conservative assessment. This was done because the sample mean is non-zero, while the GAD-B model assumes a zero-mean normal distribution for the multipath errors. Fig. 8 compares the standard deviations of true multipath errors (black-dotted line with circle markers), those corrected by the daily filter (blue-dashed line with diamond markers) and DNN (red-solid line with square markers), with the GAD-B model (magenta-solid line). All data classified as the normal cases of the selected five stations were used for the results. The standard deviations of the true multipath errors exceed the GAD-B model at the elevation bins larger than 40°. It is evident that, for this example, the CORS stations have worse environments than airports in the view of signal reflections. In contrast, the standard deviations of the multipath errors corrected by the daily filter and DNN are reasonably well-bounded by the GAD-B model. Fig. 8 also shows that the performance of the daily filter and DNN are almost the same. The fact that the DNN provides a competitive performance compared with the daily filter is consistent with the results of the reduction rate for the normal case presented in Table II.

The standard deviations of the multipath errors for the variation case are plotted in Fig. 9. The data of all dates classified as the variation case collected from the five selected stations were used to compute the standard deviations. While the true standard deviations of the multipath errors for the variation case are almost the same with those for the normal case, the standard deviations of the corrected multipath using the daily filter are increased for the variation case. This indicates that the multipath time series are different on the consecutive days, but the statistical dispersions of the magnitude of the multipath errors are at the same level. Unlike the daily filter, the performance of the DNN for the variation case is not much worse when compared to that for the normal case. It is also consistent with the results of the reduction rate for the variation case shown in Table III. It demonstrates that the multipath errors mitigated by DNN are well bounded by the ground accuracy model in both the normal and variation cases.

VII. Conclusion

A DNN based multipath empirical modeling method was introduced with the goal of capturing and estimating multipath errors of DGNSS reference stations. Testing results showed that the performance of the DNN compared better to the daily filter when the variation of the multipath error occurred due to inevitable changes in the reflecting properties of surroundings due to weather conditions. It was also demonstrated that our method when applied to degraded antenna environments could provide multipath error models which meet the GBAS standards.

The proposed method can be further extended to mitigate GNSS multipath errors of a moving platform. The multipath of a vehicle following a defined path repeatedly is expected to be modeled via machine learning techniques using geometry information between the vehicle and satellites, and the vehicle's attitude and reflecting properties. This stream of research is currently being explored as a follow-up study. Further applications to various types of DGNSS systems, including carrier phase-based systems which requires the fast and reliable solving of cycle ambiguity, can benefit from this study by mitigating multipath errors in real time.

References

[1] S. Pullen *et al.*, "Enhanced navigation, robustness, and safety assurance for autonomous vehicles as part of the globalstar connected car program," in *Proc. 31st Int. Tech. Meeting Satell. Division Inst. Navigat. (ION GNSS+)*, Oct. 2018, pp. 1538–1565.

[2] I. Greenfeld, "Concept of operations for urban air mobility command and control communications," Glenn Res. Center. Cleveland, OH, USA, Tech. Rep. 20190002633, Apr. 2019. [Online]. Available: https://ntrs.nasa.gov/citations/20190002633

[3] P. D. Groves, "Advanced satellite navigation," in *Principles of GNSS, Inertial, and Multisensor Integrated Navigation Systems*. Norwood, MA, USA: Artech House, 2008, pp. 279–302, ch. 8.

[4] C. C. Counselman, "Array antennas for DGPS," *IEEE Aerosp. Electron. Syst. Mag.*, vol. 13, no. 12, pp. 15–19, Dec. 1998, doi: 10.1109/62.735950.

[5] D. B. Thornberg, D. S. Thornberg, M. F. Dibenedetto, M. S. Braasch, F. Van Graas, and C. Bartone, "LAAS integrated multipath-limiting antenna," *Navigation*, vol. 50, no. 2, pp. 117–130, Jun. 2003, doi: 10.1002/j.2161-4296.2003.tb00323.x.

[6] L. Garin, F. van Diggelen, and J. M. Rousseau, "Strobe & edge correlator multipath mitigation for code," in *Proc. ION GPS*. Kansas City, MO, USA, Sep. 1996, pp. 657–664.

[7] H. So, G. Kim, T. Lee, S. Jeon, and C. Kee, "Modified high-resolution correlator technique for short-delayed multipath mitigation," *J. Navigat.*, vol. 62, no. 3, pp. 523–542, Jul. 2009, doi: 10.1017/S037346330900530X.

[8] M. Lashley, D. M. Bevly, and J. Y. Hung, "Performance analysis of vector tracking algorithms for weak GPS signals in high dynamics," *IEEE J. Sel. Topics Signal Process.*, vol. 3, no. 4, pp. 661–673, Aug. 2009, doi: 10.1109/JSTSP.2009.2023341.

[9] L.-T. Hsu, S.-S. Jan, P. D. Groves, and N. Kubo, "Multipath mitigation and NLOS detection using vector tracking in urban environments," *GPS Solutions*, vol. 19, no. 2, pp. 249–262, Jun. 2014, doi: 10.1007/s10291-014-0384-6.

[10] A. A. Abdallah, C.-S. Jao, Z. M. Kassas, and A. M. Shkel, "A pedestrian indoor navigation system using deep-learning-aided cellular signals and ZUPT-aided foot-mounted IMUs," *IEEE Sensors J.*, vol. 22, no. 6, pp. 5188–5198, Mar. 2022, doi: 10.1109/JSEN.2021.3118695.

[11] H.-L. Chiang, K.-C. Chen, W. Rave, M. K. Marandi, and G. Fettweis, "Machine-learning beam tracking and weight optimization for mmWave multi-UAV links," *IEEE Trans. Wireless Commun.*, vol. 20, no. 8, pp. 5481–5494, Aug. 2021, doi: 10.1109/TWC.2021.3068206.

[12] M. Yang *et al.*, "Machine-learning-based fast angle-of-arrival recognition for vehicular communications," *IEEE Trans. Veh. Technol.*, vol. 70, no. 2, pp. 1592–1605, Feb. 2021, doi: 10.1109/TVT.2021.3054757.

[13] M. Orabi, J. Khalife, A. A. Abdallah, Z. M. Kassas, and S. S. Saab, "A machine learning approach for GPS code phase estimation in multipath environments," in *Proc. IEEE/ION Position, Location Navigat. Symp. (PLANS)*, Apr. 2020, pp. 1224–1229, doi: 10.1109/PLANS46316.2020.9110155.

[14] P. Misra and P. Enge, *Global Positioning Systems: Signals, Measurements and Performances*, 2nd ed. Lincoln, MA, USA: Ganga-Jamuna Press, 2006.

[15] N. Kbayer and M. Sahmoudi, "Performances analysis of GNSS NLOS bias correction in urban environment using a three-dimensional city model and GNSS simulator," *IEEE Trans. Aerosp. Electron. Syst.*, vol. 54, no. 4, pp. 1799–1814, Aug. 2018, doi: 10.1109/TAES.2018.2801658.

[16] P. Axelrad, K. Larson, and B. Jones, "Use of the correct satellite repeat period to characterize and reduce site-specific multipath errors," in *Proc. ION GNSS*. Long Beach, CA, USA, 2005, pp. 2638–2648.

[17] D. C. Agnew and K. M. Larson, "Finding the repeat times of the GPS constellation," *GPS Solutions*, vol. 11, no. 1, pp. 71–76, Jan. 2006, doi: 10.1007/s10291-006-0038-4.

[18] K. M. Larson, A. Bilich, and P. Axelrad, "Improving the precision of high-rate GPS," *J. Geophys. Res. Atmos.*, vol. 112, no. B5, pp. 1–11, May 2007, doi: 10.1029/2006JB004367.

[19] D. Dong *et al.*, "Mitigation of multipath effect in GNSS short baseline positioning by the multipath hemispherical map," *J. Geodesy*, vol. 90, no. 3, pp. 255–262, Mar. 2016, doi: 10.1007/s00190-015-0870-9.

[20] A. K. Reichert and P. Axelrad, "Carrier-phase multipath corrections for GPS-based satellite attitude determination," *Navigation*, vol. 48, no. 2, pp. 76–88, Jun. 2001, doi: 10.1002/j.2161-4296.2001.tb00230.x.

[21] J. Guo, G. Li, Q. Kong, and S. Wang, "Modeling GPS multi- path effect based on spherical cap harmonic analysis," *Trans. Nonferrous Met. Soc. China*, vol. 24, no. 6, pp. 1874–1879, Jun. 2014, doi: 10.1016/S1003-6326(14)63266-0.

[22] C. Chen, G. Chang, N. Zheng, and T. Xu, "GNSS multipath error modeling and mitigation by using sparsity-promoting regularization," *IEEE Access*, vol. 7, pp. 24096–24108, 2019, doi: 10.1109/ACCESS.2019.2899622.

[23] Q.-H. Phan, S.-L. Tan, and I. McLoughlin, "GPS multipath mitigation: A nonlinear regression approach," *GPS Solutions*, vol. 17, pp. 371–380, Aug. 2012, doi: 10.1007/s10291-012-0285-5.

[24] Y. Lee and B. Park, "Nonlinear regression-based GNSS multipath modelling in deep urban area," *Mathematics*, vol. 10, no. 3, p. 412, Jan. 2022, doi: 10.3390/math10030412.

[25] Y. Tao *et al.*, "Real-time multipath mitigation in multi-GNSS short baseline positioning via CNN-LSTM method," *Math. Problems Eng.*, vol. 2021, pp. 1–12, Jan. 2021, doi: 10.1155/2021/6573230.

[26] D. Min, M. Kim, J. Lee, and J. Lee, "Deep neural network based multipath mitigation method for carrier based differential GNSS systems," in *Proc. ION Pacific PNT*, May 2019, pp. 451–466.

[27] *National Geodetic Survey*. Accessed: Apr. 1, 2020. [Online]. Available: https://www.ngs.noaa.gov/CORS/data.shtml

[28] NOAA. (2018). *Guidelines for New and Existing Continuously Operating Reference Stations*. [Online]. Available: https://geodesy.noaa.gov/CORS/Establish_Operate_CORS.shtml

[29] *AccuWeather*. Accessed: Jun. 1, 2019. [Online]. Available: https://www.accuweather.com/

[30] B. W. Parkinson and J. J. Spilker, "Multipath effects," in *Global Positioning System: Theory and Applications* (Progress in Astronautics and Aeronautics), vol. 1, P. Zarchan, Ed. Washington, DC, USA: American Institute of Aeronautics & Astronautics, 1996, pp. 547–568, ch. 14.

[31] C. J. Comp and P. Axelrad, "Adaptive SNR-based carrier phase multipath mitigation technique," *IEEE Trans. Aerosp. Electron. Syst.*, vol. 34, no. 1, pp. 264–276, Jan. 1998, doi: 10.1109/7.640284.

[32] M. Stinchcombe and H. White, "Multilayer feedforward networks are universal approximators," *Neural Netw.*, vol. 2, no. 5, pp. 359–366, Jun. 1988.

[33] W. Liu, Z. Wang, X. Liu, N. Zeng, Y. Liu, and F. E. Alsaadi, "A survey of deep neural network architectures and their applications," *Neurocomputing*, vol. 234, pp. 11–26, Apr. 2017, doi: 10.1016/j.neucom.2016.12.038.

[34] M. Veres and M. Moussa, "Deep learning for intelligent transportation systems: A survey of emerging trends," *IEEE Trans. Intell. Transp. Syst.*, vol. 21, no. 8, pp. 3152–3168, Aug. 2020, doi: 10.1109/TITS.2019.2929020.

[35] *Leica GNSS Networks and Reference Stations: Technical Data Hardware*, Leica Geosystems AG, Heerbrugg, Switzerland, Feb. 2011.

[36] *Trimble NetR9 GNSS Reference Receiver Data Sheet*, Trimble, Sunnyvale, CA, USA, 2013.

[37] G. A. McGraw, T. Murphy, M. Brenner, S. Pullen, and A. J. V. Dierendonck, "Development of the LAAS accuracy models," in *Proc. ION GPS*. Salt Lake City, UT, USA, Sep. 2000, pp. 1212–1223.